Minimally Interactive Knowledge-based Coronary Tracking in CTA using a Minimal Cost Path

Release 0.01

K. Krissian[1], H. Bogunović[2,3], J.M. Pozo[2,3], M.C. Villa-Uriol[2,3], A.F. Frangi[2,3]

July 8, 2008

[1]CTM, Universidad de Las Palmas de Gran Canaria, Las Palmas, Spain
[2]CISTIB, Universitat Pompeu Fabra, Barcelona, Spain
[3]Networking Center on Biomedical Research - CIBER-BBN, Barcelona, Spain

Abstract

An algorithm for minimally interactive coronary artery tracking is presented. Tracking ability and accuracy results are demonstrated on 16 images CTA images. First, a region of interest is automatically selected and a denoising filter applied. Then, for each voxel the probability of belonging to a coronary vessel is estimated from a feature space and a vesselness measure is used to obtain a cost function. The vessel starting point is obtained automatically, while the end point is provided by the user. Finally, the centerline is obtained as the minimal cost path between both points.

Latest version available at the Insight Journal [http://hdl.handle.net/1926/9999]

Contents

A minimally interactive method for the tracking of coronaries from CTA cardiac images is presented. Six independent processes (Fig. 1) constitute the proposed methodology. First a mask is generated to constrain

the execution of the algorithm to a reduced region of interest. Then, a denoising algorithm is applied to decrease noise in tissues while preserving edge sharpness. Coronaries are initially discriminated from larger vessels and the heart blood pool using a fuzzy classifier. A vesselness measure is introduced to reinforce the separation of coronaries from other non-tubular structures. A start point is automatically computed for the right and left coronaries branching from the aorta. Finally the coronary centerline is determined as the path of minimal cost connecting the start point and the manually selected end point.

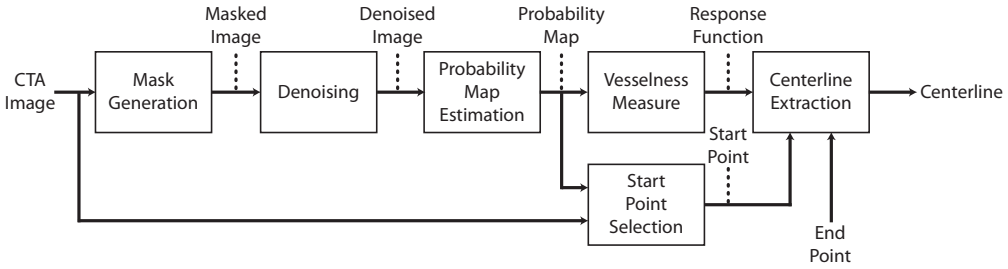

Figure 1: Coronary artery tracking workflow.

The present method aims at the successful tracking of coronary vessels while achieving a good overlap measure with the available ground-truth measurements. Accuracy of the centerline has been considered as a secondary goal for this work. This is reflected in the results section, where overlap measures are better than the accuracy ones.

1 Mask generation and denoising

First, a mask image is generated to define a region of interest using global thresholding ($-200HU$) and a binary morphological opening with a spherical structuring element of radius 3mm to remove small lung vessels.

Then, we use a denoising filter based on the Non-Local means (NL-means) algorithm [1]. The NL-means algorithm can be described by the following algorithm:

- For each voxel p of the image, consider a neighborhood $\mathcal{N}_{2t+1}(p)$ of size $(2t+1)^3$ and center at p.
- For each voxel q within $\mathcal{N}_{2t+1}(p)$ define a measure of similarity between q and p denoted as $d(q,p)$.
- Apply a transformation to the similarity $d(p,q)$ to obtain averaging weights $w(q)$ for each voxel $q \in \mathcal{N}_{2t+1}(p)$ so that the sum of the weights within the window is equal to 1. This transformation is defined as $w_p(q) = e^{-\frac{d(p,q)}{h^2}}$, where h is a threshold related to the level of noise in the image.
- Define the value of the filtered image at point p as a weighted average of the intensity values of its neighbors within $\mathcal{N}_{2t+1}(p)$ weighted by $w_p(q)$.

Specifically, in the original version of the NL-means algorithm, the distance $d(p,q)$ is defined as the $L_2 - norm$ between two windows of the same size centered at p and q. However, in practice and especially for 3D volumes, this definition is too much time consuming and we use a simpler definition that has proved still efficient both in computation time and in result quality: we use the intensity difference between a Gaussian smoothed version of the image at point p and q.

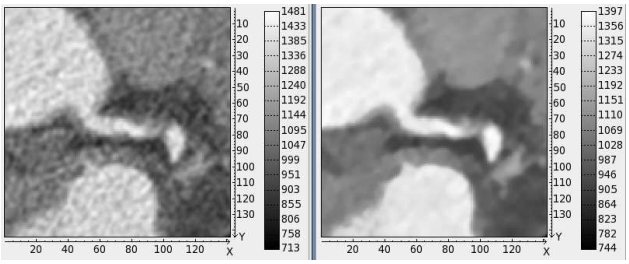

Figure 2: NL-means filter performance: (*left*) original image and (*right*) filtered image.

The central voxel p is given the weight of the maximal distance found with all the other voxels of the searching window, preventing the preservation of isolated points. The pattern similarity threshold is typically chosen as proportional to the standard deviation of the noise. In [2], the authors use $h^2 = 2\beta\sigma_n^2$, where β is a coefficient between 0.5 and 1. In all our experiments, we used the following parameters: Gaussian smoothing standard deviation of $0.4mm$, window size $t = 4$ which means 9^3 sub-windows for averaging and threshold $h = 55$.

2 Probability map estimation

Coronary vessels are distinguished from other tissue classes with a fuzzy classifier which assigns to each voxel of the image the probability of belonging to certain class of tissues. The classifier operates in the feature space which includes up to second order information in a multiscale framework. The methodology has been adapted from [4] where it was used for segmentation of cerebral vasculature.

The estimated probability map for each tissue class is a conditional probability function, $P(x \in \Re \mid \mathbf{f}(x))$, where x is a point in the image domain and $\mathbf{f}(x)$ the vector of features used to characterize the tissue at x in the estimation process. Parzen windows based on the k Nearest Neighbors rule is used for the estimation of probabilities, using $k = 25$.

The set of feature vectors belonging to a specific tissue class is first learnt in an interactive and supervised fashion from the training image data. Image content is divided into three tissue classes: blood in the coronary vessels, blood-pool inside the heart and aorta, and background, consisting of the myocardium and remaining structures. Voxels belonging to the coronary vessels are identified from 8 images where ground truth is available. All voxels within the radius minus the centerline inter-observer variability are considered as candidates for the coronary vessels. In total, 30000 points are randomly taken, equally distributed among the training images. Samples for the other two tissue classes are obtained from manual image crops around the heart. A K-means clustering algorithm ($K = 8$) was applied for non supervised tissue classification. The resulting clusters are visually examined and grouped according to the tissue class they represent. Then randomly across training data images, 30000 points are taken from the two tissue classes. As a result, the training set contains a balanced set of samples containing 30000 feature vectors per each tissue class (90000 in total).

Features are based on differential image descriptors up to the second order computed at multiple scales. The differential image descriptors used are differential invariants [8] which constitute a complete and irreducible set of differential operators for describing local image structure up to the specified order. The image intensity and the first and second-order Gaussian derivatives computed at scale σ_n. The scales are sampled exponentially: $\sigma_n = \sigma_0 e^{n\rho}$. To reduce the computational load, five scales are used ($n = [0 \ldots 4]$) leading to a 25-dimensional feature vector. For the scales to cover the size range of coronary vessels constants are set

to $\sigma_0 = 0.35$ and $\rho = 0.5$, thus covering the scales $[0.35 \ldots 2.5]$ which corresponds to the typical range of vessel radii.

Figure 3 shows examples of the estimated probability maps for the coronary vessel and blood-pool classes on image "dataset18". Brighter values indicate higher probabilities. Observing the probability map of coronary vessel class, coronary arteries have values close to 1.0. The lack of contrast causes some parts of the coronaries to have a low probability, while small areas of the contrast agent inside the heart present a high probability of being a coronary vessel.

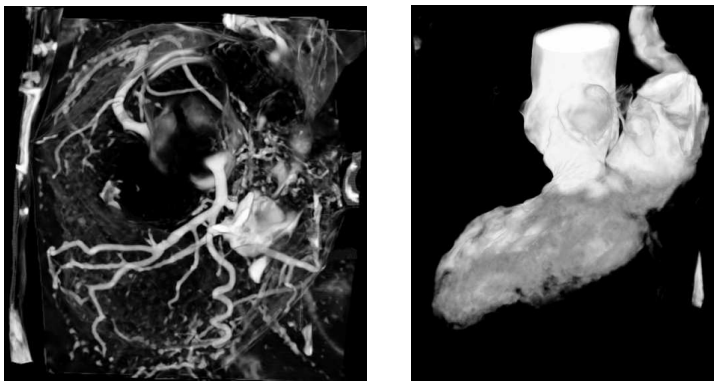

(a) Coronary vessel class. (b) Blood-pool class.

Figure 3: Volume rendering of the estimated probability maps for "dataset18".

3 Vesselness measure

A vesselness response is calculated based on [7]. The response is calculated using the coronary vessel probability map as input. In addition, the algorithm also has the following inputs: input image, minimal radius, maximal radius, number of radii and mask image.

For describing the local structure orientation, we use the same second order descriptor as presented in [3, 5, 6]. It consists in a combination of the outer product of the gradient and the squared Hessian matrix, weighted by a coefficient β, as defined by (1). The derivatives are obtained by convolution with the corresponding derivatives of a Gaussian kernel of standard deviation σ, and they are normalized using a multiplication by a factor σ^n, where n is the order of derivation, thus ensuring the scale invariance property which allows comparing responses obtained from different scales. This new operator will be denoted as $D_\sigma(I)$ and defines a local matrix at each voxel of the image, which is symmetric, real, and positive-semidefinite,

$$D(I) = \nabla I \otimes \nabla I + \beta H^2(I), \quad (1)$$

$$D_\sigma(I) = \sigma^2 \nabla_\sigma I \otimes \nabla_\sigma I + \beta \sigma^4 H^2_\sigma(I). \quad (2)$$

At each voxel, we denote $\vec{\mathbf{v}}_1, \vec{\mathbf{v}}_2$ and $\vec{\mathbf{v}}_3$ the eigenvectors of $D_\sigma(I)$ with the respective eigenvalues $\lambda_1 \geq \lambda_2 \geq \lambda_3$. For the smallest eigenvalue, the eigenvector $\vec{\mathbf{v}}_3$ gives the local direction of minimal change, which, in the case of vessels, corresponds to the local orientation of the vessel axis. In all the experiments, we set the value of β to 1.

For each scale σ, a response is computed as the mean of the boundary information along a circle in the estimated cross-section plane of the vessel. The *circle* $C_{\mathbf{x},\vec{\mathbf{v}}_1,\vec{\mathbf{v}}_2,\tau\sigma}$ is defined by its center $\mathbf{x}$, an estimate of the cross-section orientation given by the eigenvectors $\vec{\mathbf{v}}_1$ and $\vec{\mathbf{v}}_2$, and a radius proportional of the current scale

$\tau\sigma$. The *boundary information*, denoted B, is obtained with the scalar product of the gradient and the radial direction:

$$M_\sigma(\mathbf{x}) = mean_{\mathbf{y}\in C} B(\mathbf{y}) = \frac{1}{N}\sum_{i=0}^{N-1} -\sigma\nabla_\sigma I\left(\mathbf{x}+\tau\sigma\,\vec{\mathbf{v}}_\alpha\right).\vec{\mathbf{v}}_\alpha, \tag{3}$$

with $\alpha = 2\pi i/N$, and $\vec{\mathbf{v}}_\alpha = cos(\alpha)\vec{\mathbf{v}}_1 + sin(\alpha)\vec{\mathbf{v}}_2$, where N is the number of points along the circle. The gradient vector $\nabla_\sigma I$ can be computed by trilinear interpolation for better accuracy, which is especially needed when looking at small vessels.

In all the experiments, the value τ is set to $\sqrt{3}$, to maximize the selected response at the center in the case of a cylindrical circular vessel with Gaussian cross-section [7], and the number of points N around the integrating circle is set to 20.

We compute the response function M_σ for a range of scales that are discretized using a logarithmic scale in order to have more accuracy for lower scales. The minimal and maximal radius of the vessels to extract are set to 0.2 and 3.5mm respectively. The corresponding scales are calculated based on the relation between the radius r of the cylindrical circular model and the scale $\sigma(r)$ at which it gives a maximal response at the center [7]:

$$\sigma(r) = \frac{\sqrt{2}}{2}r \tag{4}$$

We typically use 6 scales for our calculations, and we denote $M_{max}(I) = \max_\sigma M_\sigma(I)$ the maximal response obtained across the scales.

4 Start point selection

For the method to be minimally interactive, two start points are automatically computed for the right and left coronaries branching from the aorta. The algorithm is summarized in 1.

Algorithm 1 Start point selection for the left and right coronary vessels.

for each image i **do**
  $coronaries$ = threshold($coronary\_probability\_map_i$, 0.95);
  $bloodpool$ = threshold($bloodpool\_probability\_map_i$, 0.95);
  cor_and_blood = threshold($coronary\_probability\_map_i + bloodpool\_probability\_map_i$, 0.95);
  s = extractTopTransverseSlice(i);
  c = detectAortaCenter(s);
  $aorta$ = regionGrowing(c, $bloodpool$);
  $aorta\_march$ = fastMarching($aorta$, cor_and_blood);
  $coronaries\_with\_distance$ = mask($aorta\_march$, $coronaries$);
  ($regionA$, $regionB$) = twoRegionsClosestToAorta($coronaries\_with\_distance$);
  $pointA$ = minDistancePoint($regionA$);
  $pointB$ = minDistancePoint($regionB$);
  if $pointA_z > pointB_z$ **then**
    $left\_coron\_start\_point = pointA$; $right\_coron\_start\_point = pointB$;
  else
    $right\_coron\_start\_point = pointA$; $left\_coron\_start\_point = pointB$;
  end if
end for

The seed point required for region growing and aorta segmentation is found from the topmost transverse slice as the center of the circle approximating cross-section of the ascending aorta. The slice image is first thresholded with value of $200HU$ and an edge is extracted. The center of the circle is found using the Hough transform with a fixed radius. The point with the highest response over the range of radii is chosen as the center of the circle. The radius range is $[14\ldots20]$mm in 0.5mm steps. The aorta is segmented with region growing within the blood-pool tissue class. Growth is limited to a 5cm range from the seed to limit the segmentation mainly to the aorta.

Starting from the already segmented aorta, a fast marching is performed within the added probability maps of two tissue classes: coronary vessels and blood-pool. Marching extends from the aorta into the heart region but also into the adjacent area of coronary vessels so that the two coronary regions closest to the aorta are identified. The segmented aorta and its further extension into coronaries is shown in Figure 4. Due to

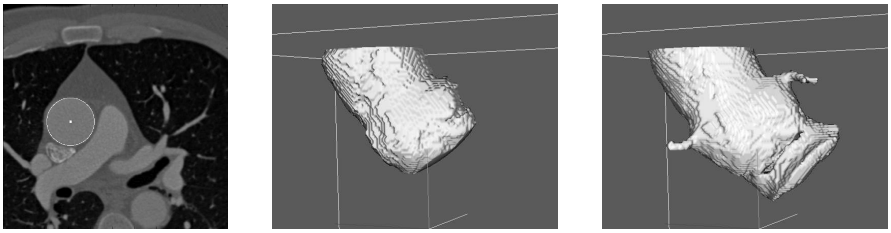

(a) Detected aorta circle is in white.

(b) Segmented aorta.

(c) Expanding from the aorta into the coronaries.

Figure 4: Aorta segmentation and later propagation into the two coronary branches.

the image acquisition, the heart is always positioned such that the start of one coronary tree is always higher in the vertical z-dimension than the other, thus enabling distinction between starting points of the left and right coronary vessels.

5 Centerline extraction using minimal cost path

For each tracked coronary its two end points are given: the automatically detected start of the left or right coronaries as described in 4, and the given endpoint, denoted E, of the aimed vessel. A path between those two points is automatically extracted maximizing the probability of being within and at the center of the searched vessel. To do so, a positive weight image W is created where maximal intensity values are given to voxels belonging to the vessels and close to their centers. A geodesic distance transform is computed by the Fast Marching algorithm, starting from the end point E, up to the initial point. To allow propagation of the front even in locations where the vesselness filter failed to detect the vessel center, we combine the vesselness response M_{max} (section 3) with the coronary vessel probability P_v (section 2) to define the weight image as:

$$W = 2M_{max} + P_v + \varepsilon, \tag{5}$$

where ε is a constant set to 0.02. This ensures that a path is always found between the two endpoints of the vessel. This path is created by backtracking the front evolution using the local intensity gradient of the geodesic distance.

6 Results

The output of the segmentation algorithm is a centerline which can be contrasted with the reference standard manually extracted by three different operators. Two different aspects are evaluated: overlap and accuracy. The results obtained for the CAT08 testing1 dataset are shown in tables 1, 2 and 3.

Dataset	**OV**			**OF**			**OT**			**Avg.**
nr.	%	score	rank	%	score	rank	%	score	rank	**rank**
8	84.5	58.7	–	80.7	65.4	–	88.3	56.7	–	–
9	74.5	60.1	–	46.1	36.2	–	74.5	49.8	–	–
10	98.1	80.4	–	90.4	71.1	–	98.2	74.1	–	–
11	84.1	63.4	–	52.7	50.2	–	84.1	55.4	–	–
12	98.3	66.7	–	31.8	18.1	–	98.9	68.3	–	–
13	94.1	72.6	–	93.5	80.5	–	95.7	72.9	–	–
14	99.3	87.3	–	83.9	82.6	–	99.3	87.1	–	–
15	99.3	85.9	–	92.0	71.6	–	99.4	87.2	–	–
16	91.4	68.0	–	89.7	80.8	–	91.7	83.3	–	–
17	91.1	80.5	–	63.2	57.1	–	91.1	60.0	–	–
18	95.1	73.0	–	78.2	74.8	–	95.1	72.6	–	–
19	79.4	77.5	–	77.8	76.7	–	79.4	77.2	–	–
20	96.3	71.3	–	58.9	47.4	–	96.3	60.8	–	–
21	98.6	63.3	–	72.7	62.8	–	99.6	74.9	–	–
22	72.1	59.2	–	25.0	25.0	–	72.3	48.6	–	–
23	97.8	86.4	–	98.0	86.5	–	97.8	86.4	–	–
Avg.	**90.9**	**72.1**	**–**	**70.9**	**61.7**	**–**	**91.4**	**69.7**	**–**	**–**

Table 1: Average overlap per dataset. The 3 metrics are *overlap* (OV), *overlap until first error* (OF) and *overlap with* $>$ 1.5*mm vessel* (OT)

Dataset	**AD**			**AI**			**AT**			**Avg.**
nr.	mm	score	rank	mm	score	rank	mm	score	rank	**rank**
8	1.14	34.3	–	0.41	38.4	–	0.87	35.5	–	–
9	16.23	21.5	–	0.38	29.9	–	18.54	21.5	–	–
10	0.43	21.7	–	0.42	22.0	–	0.43	21.6	–	–
11	1.89	25.5	–	0.42	29.9	–	1.89	25.5	–	–
12	0.38	27.7	–	0.37	28.1	–	0.38	27.7	–	–
13	0.57	28.6	–	0.35	30.2	–	0.49	29.2	–	–
14	0.38	32.0	–	0.37	32.1	–	0.38	31.9	–	–
15	0.36	28.1	–	0.35	28.2	–	0.36	28.2	–	–
16	0.69	24.4	–	0.34	26.3	–	0.71	23.2	–	–
17	0.79	47.1	–	0.35	47.9	–	0.79	47.1	–	–
18	0.52	25.6	–	0.37	26.6	–	0.52	25.6	–	–
19	4.31	27.8	–	0.52	32.8	–	4.31	27.8	–	–
20	0.49	28.7	–	0.45	29.1	–	0.49	28.7	–	–
21	0.39	23.5	–	0.37	23.7	–	0.37	23.9	–	–
22	15.29	18.3	–	0.46	24.1	–	17.22	18.3	–	–
23	0.45	28.2	–	0.39	28.6	–	0.45	28.2	–	–
Avg.	**2.77**	**27.7**	**–**	**0.39**	**29.9**	**–**	**3.01**	**27.7**	**–**	**–**

Table 2: Average accuracy per dataset. The 3 metrics are *average distance* (AD), *average distance inside vessel* (AI) and *average distance to the clinical relevant part of a vessel* (AT)

The results obtained are much better for overlap than for accuracy. This is in agreement with our main focus on recovering the most complete part of the vasculature, considering the accuracy a secondary goal. The scores obtained for overlap (table 1) are all above 58 when averaged in each dataset for the four complete centerlines (OV). This means that, in general, our algorithm behaves better than the inter-observer variability. There appear some lower ranks (cases 9, 12, 20 and 22) for *overlap until first error* (OF). It is worth to remark here that for the dataset 12, OV gives a very good percentage (98.3%) while OF is very poor (18.1). The reason is that our method detects the initial point already inside the coronary, not in the aorta. Thus, this

Measure	% / mm			score			rank		
	min.	max.	avg.	min.	max.	avg.	min.	max.	avg.
OV	0.1%	100.0%	90.9%	0.0	100.0	72.1	–	–	–
OF	0.0%	100.0%	70.9%	0.0	100.0	61.7	–	–	–
OT	0.0%	100.0%	91.4%	0.0	100.0	69.7	–	–	–
AD	0.28 mm	63.94 mm	2.77 mm	0.3	70.4	27.7	–	–	–
AI	0.28 mm	0.85 mm	0.39 mm	17.3	73.4	29.9	–	–	–
AT	0.26 mm	73.17 mm	3.01 mm	0.2	70.4	27.7	–	–	–
Total							**–**	**–**	**–**

Table 3: Summary of the results obtained for overlap and accuracy.

missing small segment will be marked as an error at the very beginning, giving a 0% in OF for this particular vessel.

In contrast with the good results for overlap, accuracy scores (table 2) are in all datasets below 50. The average score is around 28 for all accuracy measures. This means that, in general, our algorithm provides and accuracy of the order of twice the inter-observer standard deviation of the reference. However, the extremely large AD distances obtained in dataset 9 and 22 deserve an explanation. These two datasets are the only ones in which the reference vessel 3 belongs to the right coronary while we wrongly assumed that vessel 3 always belongs to the left coronary. Thus, in vessel 3 of datasets 9 and 22, our algorithm produced an alternative path from the wrong starting point until the correct end point.

References

[1] A. Buades, B. Coll, and J.M. Morel. A review of image denoising algorithms, with a new one. *Multiscale Modeling and Simulation*, 4(2):490–530, 2005. 1

[2] P. Coupé, P. Yger, S. Prima, P. Hellier, C. Kervrann, and C. Barillot. An optimized blockwise non local means denoising filter for 3D magnetic resonance images. In press. 1

[3] G. Farnebäck. *Polynomial Expansion for Orientation and Motion Estimation*. PhD thesis, Linköping University, Sweden, SE-581 83 Linköping, Sweden, 2002. Dissertation No 790. 3

[4] M. Hernandez and A.F. Frangi. Non-parametric geodesic active regions: method and evaluation for cerebral aneurysms segmentation in 3DRA and CTA. *Medical Image Analysis*, 11(3):224–241, Jun. 2007. 2

[5] K. Krissian, J. Ellsmere, K. Vosburgh, R. Kikinis, and C.-F. Westin. Multiscale segmentation of the aorta in 3d ultrasound images. In *25th Annual Int. Conf. of the IEEE Engineering in Medicine and Biology Society (EMBS)*, pages 638–641, Cancun Mexico, September 2003. 3

[6] K. Krissian and G. Farnebäck. *Medical Imaging Systems Technology: Methods in Cardiovascular and Brain Systems*, chapter Techniques in the Enhancement of 3D Angiograms and their Applications, pages 359–396. World Scientific Publishing, 2005. 3

[7] K. Krissian, G. Malandain, N. Ayache, R. Vaillant, and Y. Trousset. Model based detection of tubular structures in 3d images. *Computer Vision and Image Understanding*, 80(2):130–171, nov 2000. 3, 3

[8] B.M. ter Haar Romeny, L. Florack, J.J. Koenderink, and M.A. Viergever. Scale-space: Its natural operators and differential invariants. In *Proceedings of the 12th International Conference on Information Processing in Medical Imaging*, pages 239–255, 1991. 2